Science AAAS

Accepted Manuscript

Title: New particle formation in the free troposphere: a question of chemistry and timing

Authors: F. Bianchi[1,2,*], J. Tröstl[1], H. Junninen[3], C. Frege[1], S. Henne[4], C.R. Hoyle[1,5], U. Molteni[1], E. Herrmann[1], A. Adamov[3], N. Bukowiecki[1], X. Chen[3], J. Duplissy[6], M. Gysel[1], M. Hutterli[7], J. Kangasluoma[3], J. Kontkanen[3], A. Kürten[8], H. E. Manninen[3], S. Münch[8], O. Peräkylä[3], T. Petäjä[3], L. Rondo[8], C. Williamson[8], E. Weingartner[1,=], J. Curtius[8], D. Worsnop[3,9], M. Kulmala[3], J. Dommen[1], U. Baltensperger[1,*]

Affiliations:

[1]Laboratory of Atmospheric Chemistry, Paul Scherrer Institute, 5232 Villigen, Switzerland

[2]Institute for Atmospheric and Climate Science, ETH Zurich, 8092 Zurich, Switzerland

[3]Department of Physics, University of Helsinki, 00014 Helsinki, Finland

[4]Empa, Swiss Federal Laboratories for Materials Science and Technology, 8600 Dübendorf, Switzerland

[5]WSL Institute for Snow and Avalanche Research SLF, 7260 Davos, Switzerland

[6]Helsinki Institute of Physics, University of Helsinki, 00014 Helsinki, Finland

[7]Tofwerk AG, 3600 Thun, Switzerland

[8]Institute for Atmospheric and Environmental Sciences, Goethe-University of Frankfurt, 60438 Frankfurt am Main, Germany

[9]Aerodyne Research, Billerica, MA, 01821, USA

[=] now at: Institute for Aerosol and Sensor Technology, University of Applied Sciences (FHNW), 5210 Windisch, Switzerland

*Correspondence to: federico.bianchi@psi.ch, urs.baltensperger@psi.ch

Abstract: New particle formation (NPF) is the source of over half of the atmosphere's cloud condensation nuclei, thus influencing cloud properties and Earth's energy balance. In contrast to the planetary boundary layer (PBL), few observations of NPF in the free troposphere exist. We provide observational evidence at high altitude that, in addition to H_2SO_4-NH_3 nucleation, NPF occurs mainly through condensation of highly oxygenated molecules (HOMs). Neutral nucleation is more than ten times faster than ion-induced nucleation, and growth rates are size-dependent. NPF is restricted to a time window of 1-2 days after PBL contact of the air masses, related to the time needed for oxidation of organic compounds to form HOMs. These findings require improved NPF parameterization in atmospheric models.

One Sentence Summary: New particle formation in the free troposphere proceeds via nucleation of highly oxygenated organic compounds and is limited to a temporal window of opportunity.

Main Text:

Atmospheric aerosols influence climate through direct interaction with radiation and by acting as cloud condensation nuclei (CCN)*(1, 2)*. There is considerable uncertainty about which fraction of CCN is formed via new particle formation (NPF)(*3-5*). Studies of NPF in the free troposphere (FT) have utilized either ground-based(*6-9*) or airborne(*10*) platforms, but with limited instrumentation and/or for short time scales. Due to the lack of data at high altitudes, the vast majority of models use FT NPF schemes where particle formation rates depend only on the concentration of sulfuric acid, relative humidity, and temperature(*11*). Recently, comprehensive NPF measurements performed as part of the CLOUD experiment observed ternary nucleation of sulfuric acid with water and oxidized organics(*12*). Implementation of this NPF scheme in GLOMAP (Global Model of Aerosol Processes)(*13*) yielded a photochemically and biologically driven seasonal cycle of particle concentrations in the continental boundary layer, comparable to observations(*12*). Further CLOUD experiments observe NPF without involvement of sulfuric acid, especially in pristine regions, or the pre-industrial atmosphere(*14*). These laboratory and modeling studies call for field verification.

Here, we use a suite of state-of-the-art mass spectrometers and particle counters to chemically and physically characterize the early stage of NPF in the free troposphere, at the high-altitude research station Jungfraujoch (JFJ), Switzerland (3580 m asl, (*15*)). At this site, NPF occurs on 15-20% of the days, without apparent seasonal dependence (Fig. S9) as shown by long-term observations(*16*) and dedicated campaigns(*17*). We report measurements collected over the period of a year, including two intensive 1-month campaigns (Table S1).

We identified three typical situations represented by consecutive example days (Fig. 1); in addition, we show a special case where the sulfuric acid concentration was unusually high, ~$6 \cdot 10^6$ cm^{-3}. 25 February 2014 (Day 1) illustrates one of the many non-event days during sunny conditions. During the afternoon, there is a slight enhancement in the concentration of 5-10 nm particles, but the simultaneous increase of larger particles (up to 90 nm) suggests that this enhancement is related to vertical transport of particles formed elsewhere(*15*). 26 February (Day 2) is typical of days when the JFJ is within clouds, when NPF is suppressed by reduced global radiation and high condensation sink from the cloud droplets. Finally, 27 February and 2 March (Day 3 and 4) are two examples of NPF days, classified as 1A events(*15*), with the number concentration of particles larger than 3.2 nm ($N_{3.2}$) increasing strongly from a few hundreds to 40,000 cm^{-3}.

On most sunny days, the sulfuric acid concentration showed a similar diurnal cycle, with concentrations < 10^4 cm^{-3} during the night and ≤ $5 \cdot 10^5$ cm^{-3} during the day (except Day 4 with much higher concentrations). However, no link was found between sulfuric acid and NPF, suggesting that sulfuric acid at these concentrations does not explain NPF at the JFJ (Panel D). Instead, on some sunny days, highly oxygenated molecules (HOMs, panel D) are formed as detected with a chemical ionization-atmospheric pressure interface-time of flight mass spectrometer (CI-APi-TOF). HOM appear on certain days (e.g. Day 3), but not on other sunny days (e.g. Day 1), likely dependent on the presence of organic precursors in the FT. Panel E shows the time evolution of several negative ions measured with an atmospheric pressure interface-time of flight mass spectrometer (APi-TOF): HSO_4^-, NO_3^-, the family of clusters containing NH_3 and H_2SO_4, and ions with mass to charge ratio m/Q >400 Th, which are likely to be mainly organic compounds(*15*). Notably, nucleation nearly exclusively occurs on days where the concentration of organic compounds is high. The nucleation event on Day 4 displays a rather different ion cluster

composition; the organic ions are also present but HSO_4^- and the cluster family composed of sulfuric acid and ammonia are equally strong, probably because the sulfuric acid concentration was very high (Fig. 1). However, throughout the year of APi-TOF measurements, we never observed pure sulfuric acid clusters with more than 4 molecules (Table S3), confirming previous studies, which showed that binary H_2SO_4-H_2O nucleation does not explain atmospheric NPF(*18, 19*).

The role of HOMs is further illustrated in Fig. 2, which shows mass defect (MD) plots(*20, 21*) of negative ions for three of the days depicted in Fig. 1 (Fig. S4: corresponding neutral clusters). During the sunny day without NPF (Day 1), most ions appear at $m/Q < 300$ Th and are mainly small acid clusters. These ions appear to be spectators (ions that are always present but unlikely to participate in cluster growth, such as nitrate, oxalate and other organic acids that are too volatile to condense on such small particles). In panel B (Day 3), the smaller ions do not greatly differ from Day 1, however, many ions with $m/Q > 300$ Th are also present. The organic contribution is confirmed by the chemical composition of neutral clusters, shown in Fig. S4, S5 and Table S2. The identity of the most intense organic peaks measured by the APi-TOF overlap with those measured by the CI-APi-TOF. In both cases, we attribute these peaks to HOMs clustered with nitrate (Table S2). The difference is that in one case (ions detected by the APi-TOF) the HOMs are clustered with NO_3^- in the ambient atmosphere, while for neutral HOMs are clustered with NO_3^- inside the CI-APi-TOF ion source. Even though the chemical formulae differ from HOMs generated by monoterpene oxidation(*22-25*), they are similar in mass range and O:C ratio. They are therefore expected to have similarly low volatility and nucleating properties. Based on chemical identification of the negative ions during Day 3 (Fig. 2 and Fig. S5), the naturally charged HOMs cluster with NO_3^-, except the three most abundant peaks which also cluster to a minor extent with HSO_4^- (peaks 2a, 3a and 4a of Fig. S5). This confirms recent CLOUD findings that sulfuric acid is not important for NPF(*14*) at this concentration. On Day 4, a pronounced sequence of ions, composed of sulfuric acid and ammonia $(H_2SO_4)_m(NH_3)_nHSO_4^-$, closely resembles the sequence from purely H_2SO_4-NH_3 nucleation experiments in CLOUD(*18, 20, 21*). In addition to this family we observed other similar clusters where the charging ion is IO_3^- instead of HSO_4^- (pink dots, Fig. 2). However, as these ions are only a minor fraction of all the clusters and only a single iodate is found in the clusters we do not consider iodate to be important for this nucleation event.

On Day 3, the total particle formation rate J decreased due to the coagulation processes with increasing size, with $J_{1.6} = 51$ cm^{-3} s^{-1} and $J_2 = 46$ cm^{-3} s^{-1} (where subscripts denote mobility diameter in nm) (Fig. 3, Panel A). The formation rates of positive and negative ions with a size of 1.6 nm, determined from the neutral cluster and air ion spectrometer (NAIS) ion mode measurements, are much lower (<1 cm^{-3} s^{-1}), than those of the neutral particles for the same size, suggesting that the neutral process dominates(*26*) in this nucleation event. CLOUD results show for pure sulfuric acid nucleation a $J_{1.7}$ below 10^{-5} cm^{-3} s^{-1}(*27*) for similar concentration and temperature. There is strong indication of the presence of HOMs in the nucleating clusters, but neither of ammonia nor of amines. Since the saturation concentration is expected to decrease substantially with decreasing temperature, we consider this to be in good agreement with Kirkby et al.(*14*), who reported $J_{1.7} = 40$ cm^{-3} s^{-1} at [HOM] = $4 \cdot 10^8$ cm^{-3} and $T = 5$°C.

On Day 4, the observed $J_{3.2}$ of ~4.5 cm^{-3} s^{-1}, at temperatures between -12°C and -15°C, was similar to that measured at CLOUD, $J_{1.7} \sim 4$ cm^{-3} s^{-1} for [H_2SO_4] = $6 \cdot 10^6$ cm^{-3} and [NH_3] = 1 ppbv at T = -15°C(*18*). As the ammonia concentration during this event at the JFJ is expected to be lower than 1 ppbv, we hypothesize a synergistic effect of H_2SO_4, NH_3 and non-negligible concentrations of

HOMs. Note that this was a special case where the sulfuric acid concentration was extremely high. However, HOMs were present in the initial clusters in 13 out of 19 nucleation events (type 1A or 1B), as observed with the APi-TOF (shown in Table S3). Nucleation thus appears to be influenced by the presence of organic compounds in the majority of cases. The importance of HOMs is further illustrated by the size-dependent growth rates (GR) observed during particle formation (Fig. 3), giving confirmation of nano-Köhler growth(*3*) also for FT conditions. On Day 3, the GR is initially driven by HOMs, and continues to increase after the HOMs concentration begins to decline, likely due to a reduced Kelvin effect at larger particle sizes, enabling the condensation of more volatile (un-measured) molecules (Fig. S8)(*28*). On Day 4, a greater part of the initial growth rate is explained by sulfuric acid and water under the assumption of condensation at the kinetic limit (Fig. S7)(*29*). After that, the higher growth rate cannot be explained by sulfuric acid alone, again likely indicative of condensation of more volatile (un-measured) molecules(*30*) on the newly formed particles in this case, showing that this process is also not entirely inorganic.

An important question is where the condensable vapors or their precursors originate. We used the Lagrangian Particle Dispersion Model FLEXPART in time-inverse mode and compared air mass origins of all the major events (1A and 1B) to typical non-event days during the same period(*15*). Increases in simulated carbon monoxide (CO) concentration and source receptor relationship (SRR), indicative of planetary boundary layer (PBL) influence, along individual backward simulations were established (Fig. 4 and S10). This suggests an anthropogenic source of the HOM precursors but does not preclude a biogenic source. For all simulated cases, the small increase in CO within 6 hours before arrival suggests no significant influence from local emissions during this period. Air masses experienced enhanced uptake of CO and also an increase in SRR (Fig. S11) 12 to 40 hours before Type 1A events detected at the JFJ, caused by contact with polluted boundary layer air. Similarly, air masses connected to 1B events showed increased CO uptake, however, somewhat further upwind, between 12 to 72 hours before arrival at the JFJ, with a maximum uptake at 48 hours. In contrast, for non-event days (NON), CO uptake was significantly below that during nucleation events. This indicates that one requirement for observing NPF at the JFJ is non-local (Fig. S12) contact with the PBL and, hence, the uptake of emissions hours before arrival at the JFJ, resulting in a sufficiently long processing time in the free troposphere. An optimal transport time from the PBL to foster nucleation appears to be around 1 day, while longer transport times result in less clear nucleation events, due to ongoing oxidation and dilution of the precursor gases.

Combining in-situ observations and modeling results, we thus find that NPF in the free troposphere depends on the availability of highly oxidized organic species, providing observational evidence for NPF pathways seen in recent laboratory experiments. The availability of these highly oxidized organic species in turn is found to depend on previous surface contact of the air mass and the appropriate time to process the precursors from the boundary layer on their way up. In short, chemistry and timing play the main roles. To properly represent nucleation in the free troposphere, future atmospheric models should take these factors into account.

References and Notes:

1. T. L. Anderson *et al.*, *Bull. Amer. Meteor. Soc.* **86**, 1795-1809 (2005).
2. R. J. Charlson *et al.*, *Science* **255**, 423-430 (1992).
3. M. Kulmala *et al.*, *J. Aerosol Sci.* **35**, 143-176 (2004).
4. J. Merikanto, D. V. Spracklen, G. W. Mann, S. J. Pickering, K. S. Carslaw, *Atmos. Chem. Phys.* **9**, 8601-8616 (2009).

5. R. Y. Zhang, A. Khalizov, L. Wang, M. Hu, W. Xu, *Chem. Rev.* **112**, 1957-2011 (2012).
6. S. Rodríguez *et al.*, *Atmos. Chem. Phys.* **9**, 6319-6335 (2009).
7. C. Rose *et al.*, *Atmos. Environ.* **102**, 18-29 (2015).
8. H. Venzac *et al.*, *Proc. Natl. Acad. Sci. USA* **105**, 15666-15671 (2008).
9. F. Q. Yu, A. G. Hallar, *J. Geophys. Res.-Atmos.* **119**, 12246-12255 (2014).
10. S. Mirme *et al.*, *Atmos. Chem. Phys.* **10**, 437-451 (2010).
11. M. Kulmala, A. Laaksonen, L. Pirjola, *J. Geophys. Res.-Atmos.* **103**, 8301-8307 (1998).
12. F. Riccobono *et al.*, *Science* **344**, 717-721 (2014).
13. G. W. Mann *et al.*, *Geosci. Model Dev.* **3**, 519-551 (2010).
14. J. Kirkby, *Submitted*, (2016).
15. *Materials and methods are available as supplementary materials on Science Online.*
16. E. Herrmann *et al.*, *J. Geophys. Res.-Atmos.* **120**, 9459-9480 (2015).
17. J. Boulon *et al.*, *Atmos. Chem. Phys.* **10**, 9333-9349 (2010).
18. J. Kirkby *et al.*, *Nature* **476**, 429-433 (2011).
19. F. L. Eisele *et al.*, *J. Geophys. Res.-Atmos.* **111**, 11 (2006).
20. F. Bianchi *et al.*, *Environ. Sci. Technol.* **48**, 13675-13684 (2014).
21. S. Schobesberger *et al.*, *Proc. Natl. Acad. Sci. USA* **110**, 17223-17228 (2013).
22. M. Ehn *et al.*, *Nature* **506**, 476-479 (2014).
23. T. Jokinen *et al.*, *Proc. Natl. Acad. Sci. USA* **112**, 7123-7128 (2015).
24. T. F. Mentel *et al.*, *Atmos. Chem. Phys.* **15**, 6745-6765 (2015).
25. M. P. Rissanen *et al.*, *J. Am. Chem. Soc.* **136**, 15596-15606 (2014).
26. C. Rose *et al.*, *Atmos. Chem. Phys.* **15**, 3413-3428 (2015).
27. J. Duplissy *et al.*, *J. Geophys. Res.-Atmos.* **121** (2015) doi: 10.1002/2015JD023539.
28. M. Kulmala *et al.*, *Science* **339**, 943-946 (2013).
29. T. Nieminen, K. E. J. Lehtinen, M. Kulmala, *Atmos. Chem. Phys.* **10**, 9773-9779 (2010).
30. T. Berndt *et al.*, *J. Phys. Chem. A* **119**, 10336-10348 (2015).
31. U. Baltensperger *et al.*, *J. Geophys. Res.-Atmos.* **102**, 19707-19715 (1997).
32. E. Weingartner, S. Nyeki, U. Baltensperger, *J. Geophys. Res.-Atmos.* **104**, 26809-26820 (1999).
33. N. Bukowiecki *et al.*, *Aerosol Air Qual. Res.* (2016) doi: 10.4209/aaqr.2015.05.0305.
34. J. Vanhanen *et al.*, *Aerosol Sci. Tech.* **45**, 533-542 (2011).
35. K. Lehtipalo *et al.*, *Boreal Environ. Res.* **19**, 215-236 (2014).
36. S. C. Wang, R. C. Flagan, *Aerosol Sci. Tech.* **13**, 230-240 (1990).
37. E. O. Knutson, K. T. Whitby, *J. Aerosol Sci.* **6**, 443-451 (1975).
38. S. Mirme, A. Mirme, *Atmos. Meas. Tech.* **6**, 1061-1071 (2013).
39. N. Hyttinen *et al.*, *J. Phys. Chem. A* **119**, 6339-6345 (2015).
40. A. Kurten, L. Rondo, S. Ehrhart, J. Curtius, *J. Phys. Chem. A* **116**, 6375-6386 (2012).
41. R. Fröhlich *et al.*, *Atmos. Chem. Phys.* **15**, 11373-11398 (2015).
42. M. Kulmala *et al.*, *Nat. Protoc.* **7**, 1651-1667 (2012).
43. J. H. Seinfeld, S. N. Pandis, *Atmospheric Chemistry and Physics: From Air Pollution to Climate Change*. 2nd Edition, (J. Willey, New York, 2006).
44. H. E. Manninen *et al.*, *Boreal Environ. Res.* **14**, 591-605 (2009).
45. A. Hirsikko *et al.*, *Atmos. Chem. Phys.* **11**, 767-798 (2011).
46. K. E. J. Lehtinen, M. Kulmala, *Atmos. Chem. Phys.* **3**, 251-257 (2003).
47. N. A. Fuchs, A. G. Sutugin, *Highly Dispersed Aerosols*, (Ann Arbor Science Publishers, London, 1970).
48. P. A. Baron, K. Willeke, *Aerosol Measurement: Principles, Techniques, and Applications*, (Wiley-Interscience, 2001).
49. A. Stohl, C. Forster, A. Frank, P. Seibert, G. Wotawa, *Atmos. Chem. Phys.* **5**, 2461-2474 (2005).
50. P. Seibert, A. Frank, *Atmos. Chem. Phys.* **4**, 51-63 (2004).
51. D. Brunner *et al.*, in *Lagrangian Modeling of the Atmosphere,* J. Lin, D. Brunner, C. Gerbig, A. Stohl, A. Luhar, P. Webley, Eds. (American Geophysical Union, Washington, 2012), vol. 200, pp. 207-221.
52. C. A. Keller *et al.*, *Geophys. Res. Lett.* **38**, 5 (2011).
53. M. I. Garcia, S. Rodriguez, Y. Gonzalez, R. D. Garcia, *Atmos. Chem. Phys.* **14**, 3865-3881 (2014).
54. E. Jarvinen *et al.*, *Atmos. Chem. Phys.* **13**, 7473-7487 (2013).
55. K. Neitola *et al.*, *Atmos. Chem. Phys.* **11**, 8447-8458 (2011).
56. J. Boulon *et al.*, *Atmos. Chem. Phys.* **11**, 5625-5639 (2011).

57. A. G. Hallar, D. H. Lowenthal, G. Chirokova, R. D. Borys, C. Wiedinmyer, *Atmos. Environ.* **45**, 4111-4115 (2011).

Acknowledgments:

We thank the International Foundation High Altitude Research Stations Jungfraujoch and Gornergrat for the opportunity to perform experiments on the Jungfraujoch and especially the research station's custodians Joan and Martin Fischer, Maria and Urs Otz for their support and hospitality. This work was supported by the Swiss National Science Foundation (200020_135307, 20020_152907, 206021_144947, 200021_140663), by MeteoSwiss in the framework of the Global Atmosphere Watch program and FP7 project ACTRIS (grant agreement no. 262254). Funding was also received from the Academy of Finland Centre of Excellence (grant no. 272041, 1118615), the EC Seventh Framework Program (Marie Curie Initial Training Network MC-ITN "CLOUD-TRAIN" no. 316662), the German Federal Ministry of Education and Research (project no. 01LK1222A), the FP7 project BACCHUS (grant agreement no. 603445) and the ERC, under grant 615922-BLACARAT. We thank the tofTools team for providing tools for mass spectrometry analysis.

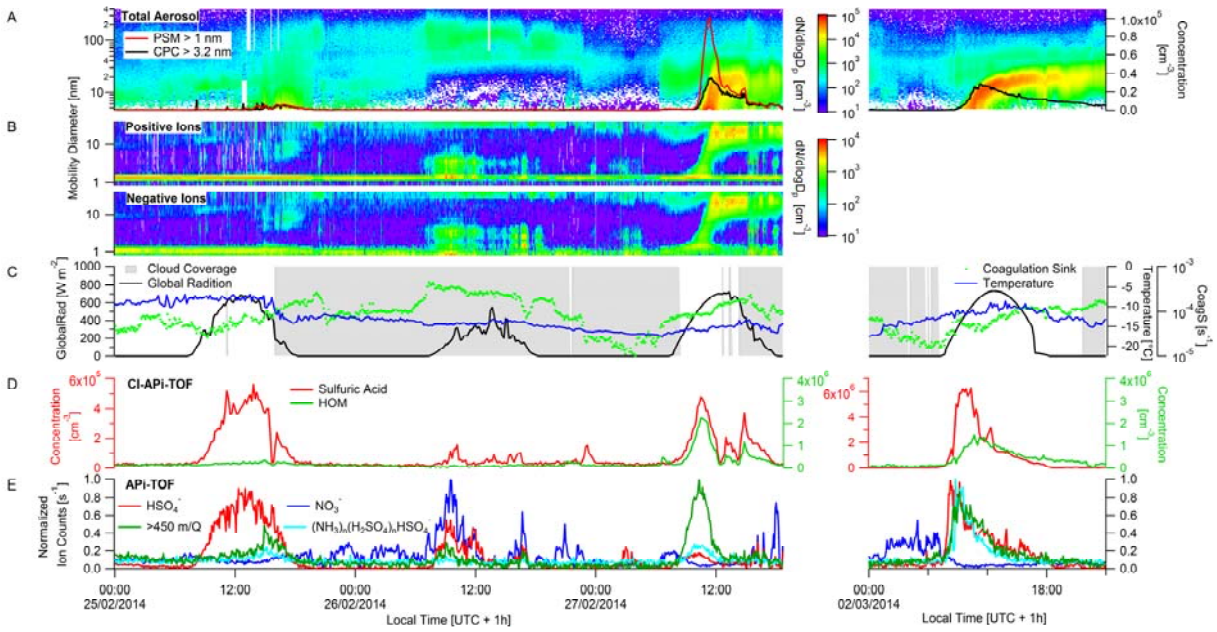

Fig. 1. Four representative situations observed at the JFJ between 25-27 February and on 2 March 2014. Sunny day with no nucleation (25 February - Day 1); cloudy day (26 February - Day 2); nucleation day with HOMs (27 February - Day 3); nucleation day with H_2SO_4, NH_3 and HOMs (02 March - Day 4). (A) Particle size distribution and particle number concentration above 1 and 3.2 nm measured with the nano-SMPS, PSM, and CPC respectively. (B) Size distributions of the positive and negative ions from a neutral cluster and air ion spectrometer (NAIS). (C) Global radiation, coagulation sink and cloud coverage. (D) Concentrations of sulfuric acid (red) and HOMs (green) measured with the CI-APi-TOF. Note the different axis for sulfuric acid in the right panel. (E) Measurements of specific ions with the APi-TOF, HSO_4^- in red, NO_3^- in blue, sum of m/z > 450 Th in green. The clusters containing sulfuric acid and ammonia are shown by a light blue line.

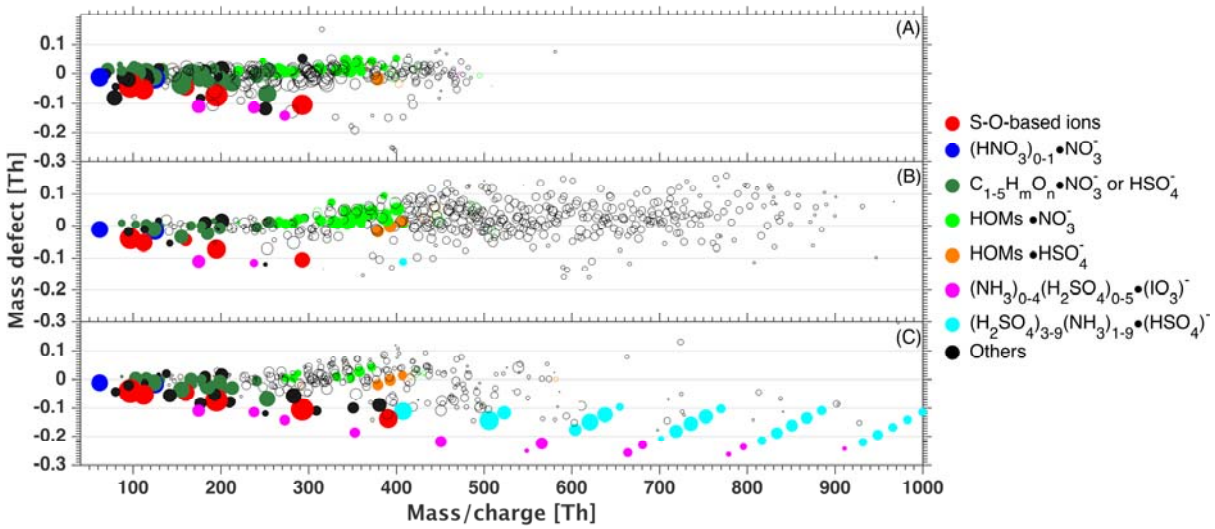

Fig. 2. Mass defect (MD) plots (negative ions) measured on (A) Day 1, (B) Day 3 and (C) Day 4. The abscissa presents the mass-to-charge ratio and the ordinate the mass defect, which is the difference between the nominal (integer) mass and the exact mass. Colors relate to pure sulfuric acid clusters (red), nitrate (blue), small organic compounds alone or clustered with NO_3^- or HSO_4^- (dark green), HOMs clustered with NO_3^- (light green), HOMs clustered with HSO_4^- (orange), H_2SO_4-NH_3 clusters (light blue) and H_2SO_4-NH_3-HIO_3 (pink). The marker size is proportional to the logarithm of the count rate. The mass spectra for the same events are reported in Fig. S3.

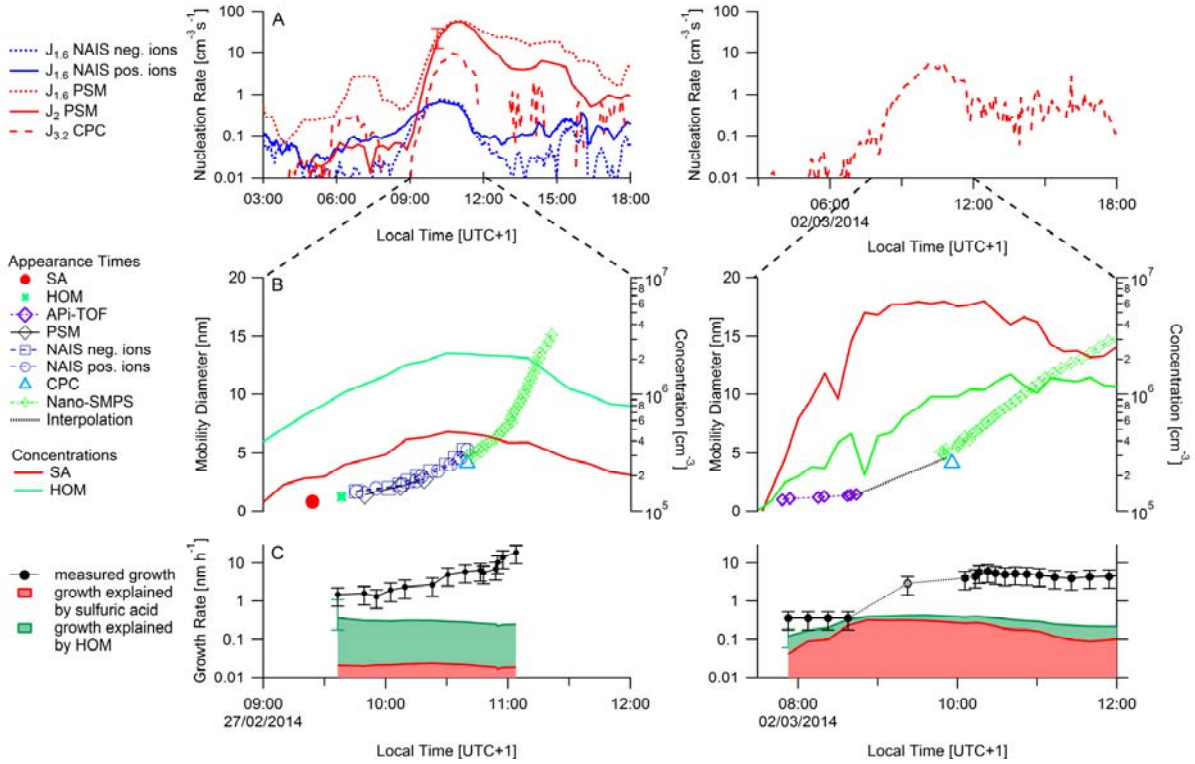

Fig. 3. Particle evolution during the nucleation events observed on Day 3 and Day 4. Panel A: Formation rates of the particles and ions at different sizes. Panel B: Evolution of particle diameter during the nucleation events. The two solid lines (red and green) show the concentrations of sulfuric acid and the HOMs. Panel C: Comparison of the measured growth rates with growth rates as calculated when assuming that solely sulfuric acid contributes to the growth(*29*) in red and including also HOMs in green. Besides having a much higher sulfuric acid concentration, Day 4 shows a $J_{3.2}$ and a GR that are slightly lower. On that day, not all instruments to measure the particles all the way from 1 nm to 15 nm were functioning. Therefore the growth rate was interpolated between approximately 08:40 and 10:00.

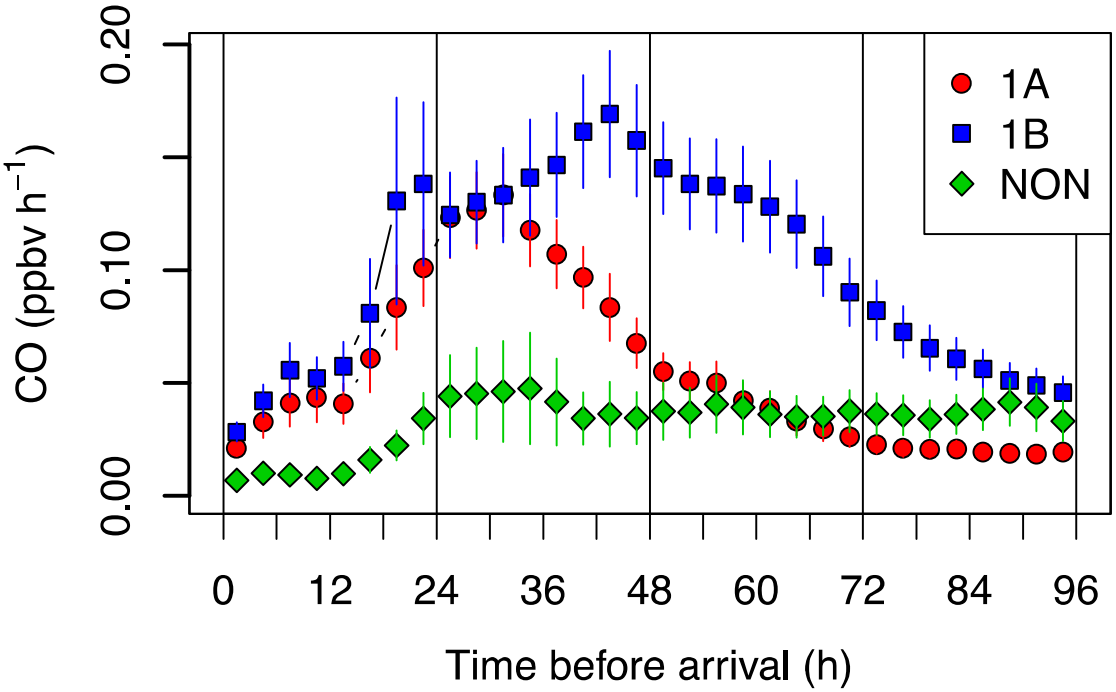

Fig. 4. Simulated mean and standard uncertainty of the mean (error bars) for anthropogenic-carbon monoxide (CO) uptake versus time before arrival at JFJ, for air masses sampled under different nucleation conditions: 1A events (red) pronounced and clearly identifiable events, 1B events (blue) less well defined nucleation events and NON (green) no nucleation events.

Supplementary Materials:

Materials and Methods

Figures S1-S12

Tables S1-S4

Author Information: The authors declare no competing financial interests. Correspondence and requests for materials should be addressed to Federico Bianchi (federico.bianchi@psi.ch) or Urs Baltensperger (urs.baltensperger@psi.ch).